Annals of Nuclear Medicine Vol. 5, No. 1, 1–9, 1991

Quantitative measurement of uptake of radiolabeled monoclonal antibody by means of planar data

Yoshihisa AKIYAMA,* Nobuharu YUI,** Toru MATSUMOTO,*** Takeshi A. IINUMA,*** Hiroo IKEHIRA,*** Hiroshi FUKUDA*** and Yukio TATENO***

*Physics Division, **Division of Nuclear Medicine, Chiba Cancer Center Hospital
***Division of Clinical Research, National Institute of Radiological Science

Data obtained from planar images were used to measure the uptake of monoclonal antibody in organs and tumors. Background counts included in the region of interest were eliminated, and the attenuation of the photons emitted by the radionuclide through the intervening tissues was compensated for. The background counts and the intensity of the attenuation were determined from the results of phantom studies and numerical integration with a personal computer. The quantitative uptake of ^{111}In labeled anti-melanoma Monoclonal Antibody (ZME-018) in a melanoma lesion, the liver, and the bone marrow of a patient was measured by the planar method which we developed.

Key words: monoclonal antibody, dosimetry, planar data, numerical integration, background subtraction

INTRODUCTION

The USE OF RADIOLABELED monoclonal antibodies (MoAbs) in cancer therapy is one of the most attractive new treatment approaches, and its clinical utility will be established in the near future.[1–3] To support this clinical utility, dosimetry for organs and tumors is indispensable.[3] It is particularly important to assess the limiting absorption dose in target organs as well as the effective absorption dose in the tumor. There are two methods for measuring radioactive quantities in organs and tumors: Single Photon Emission Computed Tomography (SPECT) and planar methods.[3] Since SPECT can give the three-dimensional distribution of radioactivity, it is possible to associate the reconstructed values with the radioactivity levels.[4–6] SPECT, however, presents some difficulties with respect to attenuation correction in actual clinical cases. Since the number of counts obtained from immunoscintigraphy is generally small, statistical error in image processing for reconstruction is a problem.[7] Furthermore, as the reconstruction algorithm greatly amplifies the effects of camera and collimator nonuniformity, the radioactivity obtained by SPECT might possibly contain a great degree of error.[8] For these reasons, great care is necessary in measuring the radioactive quantity by SPECT. As an alternative, there is the planar method. This method, developed by Sorenson[9] and others,[10–15] uses both anterior and posterior data. If the organ or tumor portion is close to the abdomen or dorsal skin, the planar data obtained from the opposite side detector of the portion contain significant noise, because the count emitted by the organ or tumor portion is attenuated considerably through the intervening tissue. Hence, we do not believe that planar data from the opposite side of the portion are useful in calculating the uptake if the portion is close to the abdomen or dorsal skin. For these reasons, when the organ or tumor portion was close to the abdominal or dorsal skin, only the planar data proximal to the portion were used. In any case, background subtraction[16] and attenuation compensation are indispensable. The background counts and

Received April 24, 1990, revision accepted August 22, 1990.

For reprints contact: Yoshihisa Akiyama, Physics Division, Chiba Cancer Center Hospital, 666–2, Nitonocho, Chiba-shi 280 JAPAN.

the intensity of the attenuation were computed by numerical integration for individual organ and tumor portions.

MATERIALS AND METHODS

Normally, both anterior and posterior data were used. Radioactivity was determined with formula (1) in the case of both anterior and posterior data.

$$\beta \times \sqrt{C_1 \cdot AC_1 \times C_2 \cdot AC_2} \qquad (1)$$

where β is a conversion constant for converting from cpm units to mCi units; C_1 and C_2 are counts (cpm) emitted from the organ or tumor in the anterior and posterior regions of interest (ROI); and AC_1 and AC_2 are correction values to correct the attenuation in the body for anterior and posterior data, respectively.

Radioactivity was determined with formula (2) when one side data were used.

$$\beta \times C \cdot AC \qquad (2)$$

where C is the cpm emitted by the organ or tumor in the ROI and AC is the correction value to correct the attenuation in the body.

When a point source is attenuated in material with a uniform attenuation coefficient, the correction values AC_1, AC_2, and AC can be obtained easily with formula (3).

$$1/e^{-\mu l} \qquad (3)$$

where μ and l are the linear attenuation coefficient and the path length in the absorber, respectively. However, it is not so easy to calculate the correction value for an actual human organ and tumor, because its shape is generally complex. It is possible to calculate the correction value by using numerical integration (Appendix 1) when the three-dimensional distribution of the attenuation coefficient and the organ outline can be obtained and the radioactivity per unit volume within the organ (tumor) is uniform.

Background counts from outside the organ (tumor) and from portions superimposed on the organ (tumor) are included within the organ (tumor) ROI. These background influences were selected and discarded by means of the calculations described in Appendix 2.

A GE (Milwaukee, U.S.A.) Maxi Camera 400 AC equipped with a medium energy parallel hole collimator was used to collect the data in the phantom experiment and clinical study. Photopeaks of ^{111}In both at 172 KeV and 247 KeV with window settings of 20% were selected.

The clinical case reported here was a female patient with melanoma in the left femoral region. Twenty mg of ZME-018 was labeled with 129.5 MBq (3.5 mCi) ^{111}In and injected intraveneously.

Images were taken on the day of the injection, and 1, 2, 3, and 5 days after. On the day of the injection, no image of the femoral region was able to be obtained. The collection of imaging data was done on a 128×128 matrix, and the exposure time was 5 minutes.

RESULTS

A. Phantom experiment

Preceding the actual clinical measurements, the conversion constant β and the attenuation coefficient μ, which are necessary for computation, were determined in a phantom experiment. A ^{111}In point source was fixed at several places on the collimator surface to eliminate non-uniformity of the detector system. We calculated the β value to be 1.75×10^{-6} mCi/count.

The attenuation coefficient was determined from changes in the counts of incident radiation measured with the detector by varying the water volume (thickness) in a polystyrene tank that was placed between the ^{111}In point source and the detector. The results are plotted in Fig. 1. The relation between the points on the semi-logarithmic graph was approximately linear with a slope of -0.1 cm^{-1}, so the linear attenuation coefficient was set at 0.1 cm^{-1}.

B. Clinical study

Using planar data that were fed into a computer, we calculated the uptake ratio of the injection dose per unit weight of the tumors in the left femoral region, as well as in the liver and the bone marrow, which are thought to be critical tissues for treatment.

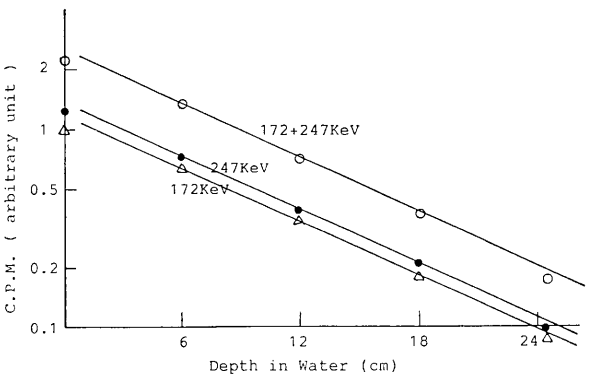

Fig. 1 Attenuation of ^{111}In in water Twenty-percent windows were centered over 172 and 247 KeV photo peaks. The horizontal axis shows the depth of water that was passed through, and the vertical axis is the relative count which is shown on a logarithmic scale. The attenuation coefficient for the double windows was -0.1 cm^{-1}. Attenuation coefficients for the single window were similar to that for the double window.

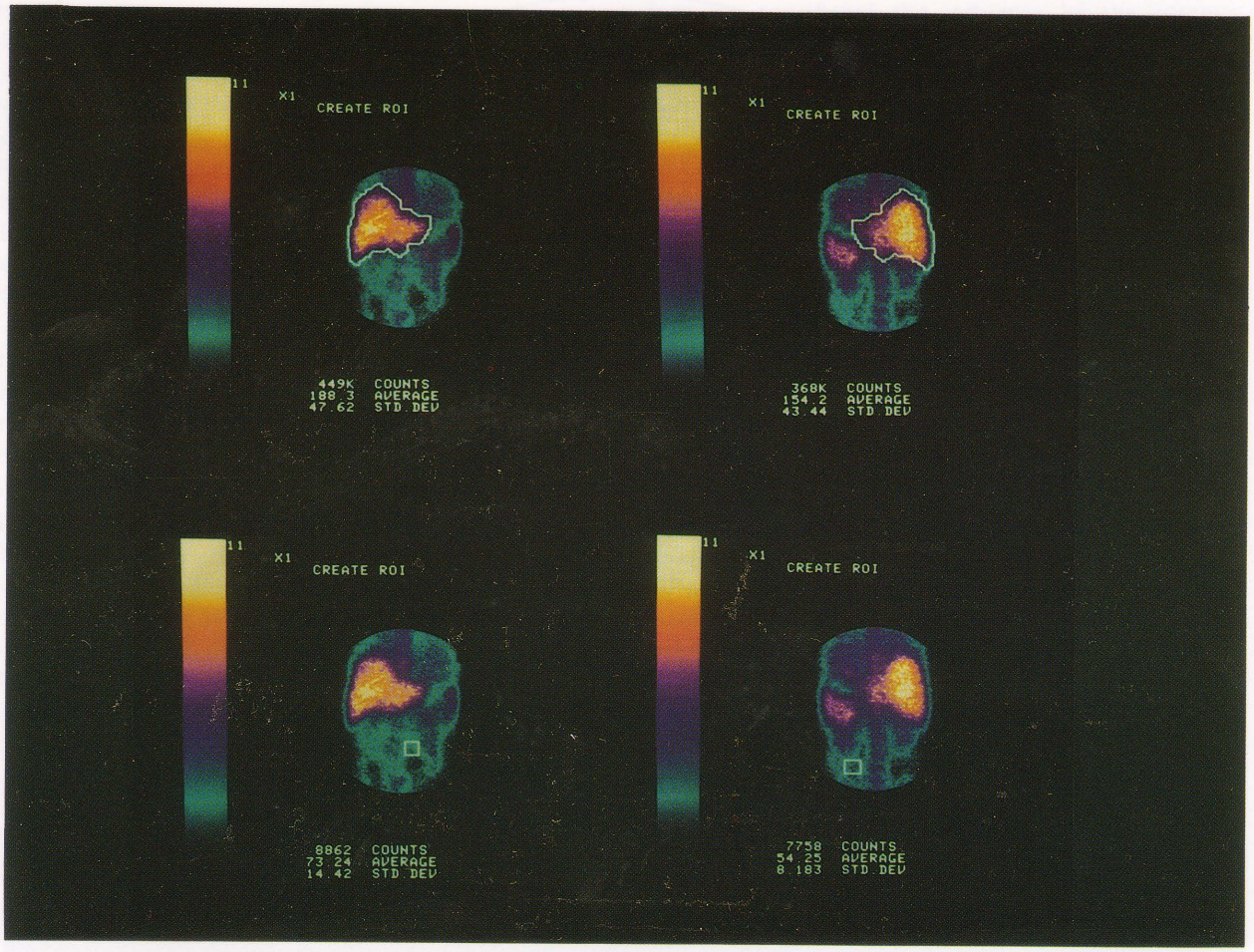

Fig. 2 Immunoscintigrams of the abdominal region. Left sides are anterior and right sides are posterior views. The upper row images represent liver ROIs for the calculation of liver uptake. The lower row images represent the background ROIs which served as a reference in eliminating the background activity included in the liver ROI. The same ROI was used from the day of injection to 5 days after injection.

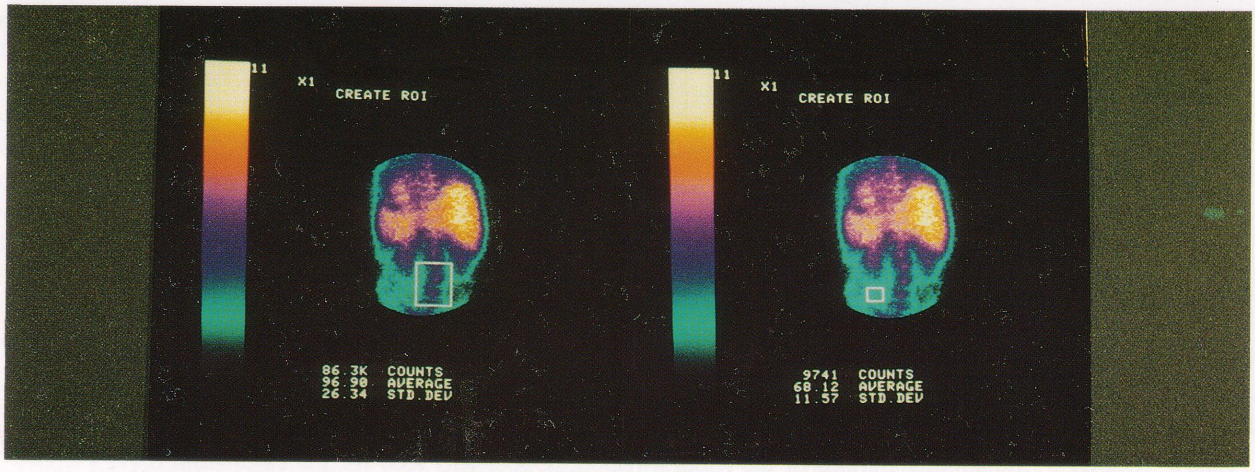

Fig. 3 Immunoscintigrams of the bone marrow region. ROI in the left side image was used in calculating the bone marrow uptake and that in the right side image was served as a reference in eliminating the background count included in the bone marrow ROI.

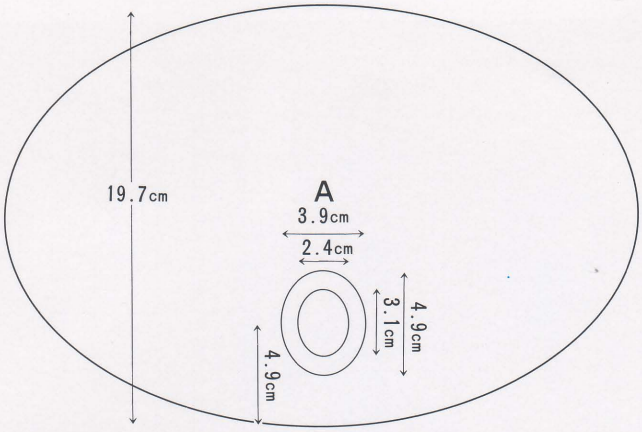

Fig. 4 Estimated transverse section of bone marrow region. The spinal column is the same as that of the average Japanese man. The bone marrow was thought to be in the center of the spinal column, and its size was calculated on the basis of the ratio[17] of the weight of bone to bone marrow. The calculated volume of bone marrow was taken to be 0.39 times that of the spinal column. Some γ-rays within region "A," 3.9 cm, pass through the osseous matter portion, so the values used in correcting the attenuation and the background counts within each pixel of region "A" were calculated by numerical integration in due consideration of these effects.

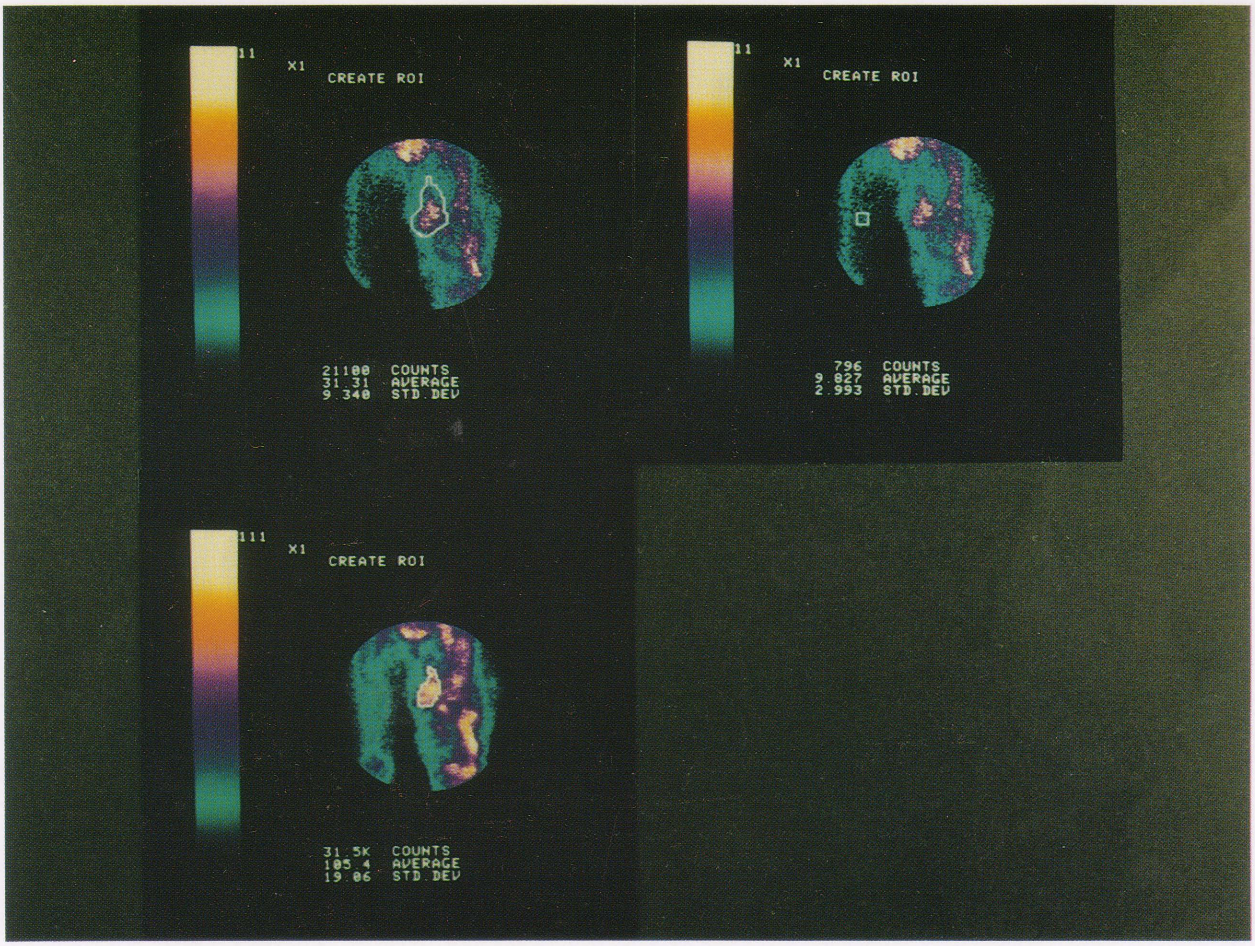

Fig. 5 Immunoscintigrams of the femoral region. (Upper left) ROI for the calculation of tumor uptake. Its size was greater than the surface area of the tumor because of the low resolution of detector system. (Upper right) ROI for the calculation of the background level included in the tumor ROI. (Lower left) ROI for the determination of the surface area of the tumor.

1. Liver

Based on the data from both the upper and lower planar images, uptake in the liver was calculated with formula (1). The liver ROI and the ROI used for calculating the background count are shown in Fig. 2. In this paper we assumed for simplicity that the subject's liver and body size were the same as those of the average Japanese man,[17] which was reduced on the basis of the data for the MIRD standard man.[18]

The liver ROI included background counts from outside the liver and from portions superimposed on the liver. We determined the background count included in the liver ROI with Appendix 2 on two assumptions: that the liver ROI was drawn outside one centimeter from the boundary of the liver, and that the radioactive concentration superimposed on the liver and outside the liver in the liver ROI was equal to that for the background ROI. Calculating from Appendix 2, the mean background count per pixel included in the anterior and posterior liver ROI was 66% and 75% of the mean count per pixel for the anterior and posterior background ROI, respectively. The 66% count per pixel for the anterior background ROI was subtracted from the count for each pixel in the anterior liver ROI. In a similar way, the 75% count per pixel for the posterior background ROI was also subtracted from the count for each pixel in the posterior liver ROI. Attenuation due to the tissue was then corrected. The correction values, AC_1 and AC_2 in formula (1), were calculated to be 1.9 and 2.54, respectively, according to Appendix 1.

2. Bone marrow

The bone marrow ROI and the ROI that was used to calculate the background levels in the bone marrow ROI are shown in Fig. 3. Since the bone marrow is close to the dorsal skin, and it barely appeared in the anterior view images, only the posterior data were used. The calculation was therefore performed with formula (2). The hypothetical anatomical locations of bone marrow[22] are shown in Fig. 4. The linear attenuation coefficients we used were 0.1 cm^{-1} of water as non-osseous matter, and 0.15 cm^{-1} as the osseous matter. As the background counts from outside the bone marrow were included in the bone marrow ROI, we assumed that background radioactive concentrations were the same as that for the background ROI, and then these background counts were subtracted from the count for the bone marrow ROI.

These background counts were computed on the basis of Appendix 2. (Appendix 2 was derived on the assumption that the attenuation coefficient was uniform. But the γ-ray incident in the bone marrow ROI passes through the osseous portion, and therefore we considered the influence of the osseous portion. The pass length, lon, was divided into two parts: lons for the osseous matter, and lont for the non-osseous matter. The expression in parenthesis in the equation (A) was changed to $e^{-0.15\times lo_1s-0.1\times lo_1t} + \cdots + e^{-0.15\times lons-0.1\times lont}$. Also the expression of the numerator in the brace of equation (B) was changed to the same form.) We obtained the following results: Each pixel in region "A" in Fig. 4 which is influenced by the spinal column included 82% of the mean pixel count for background ROI. So, 82% of the count per pixel of the background ROI was subtracted from the count for each pixel in region "A" in Fig. 4. Attenuation correction was performed with formula (2). In this calculation, we used 1.56 as the correction value AC in formula (2), which was computed on the basis of Appendix 1. (For the bone marrow portion, $e^{-\mu l_1}$, $\cdots$ and $e^{-\mu l_n}$ in Appendix 1 were changed. The pass length, l_n, was divided into two parts: that of osseous matter, l_{ns}, and that of non-osseous matter, l_{nt}. The expressions $e^{-\mu l_1}$, $\cdots$ and $e^{-\mu l_n}$ in Appendix 1 were then changed to $e^{-0.15\times l_1s-0.1\times l_1t}$, $\cdots$ and $e^{-0.15\times l_{ns}-0.1\times l_{nt}}$, respectively.)

3. Tumor portion of the left femoral region

Figure 5 shows scintigrams of the femoral region showing a large tumor in the left femoral. Since the tumor was located in the anterior surface, we calculated the radioactivity with formula (2) using the data from the anterior view image only. Since there were numerous tumors of various sizes ranging up to a diameter of 3 cm at this location, we calculated the radioactivity according to two types of models, in which the tumor extended 5 mm below the skin and in which the tumor extended to a depth of 3 cm below the skin. Furthermore, we calculated on the assumption that the radioactive concentration of the background portions superimposed on the tumor was equal to that of right femoral region, which was chosen as background material. The thickness of both femoral regions was thought to be 10 cm.

The calculation procedure was the same as those for the liver and the bone marrow. The background count in tumor ROI was subtracted, and then attenuation due to the tissue was corrected.

Table 1 Percent uptake per gram of tissue

Days after injection	0	1	2	3	5
Liver	0.009	0.0088	0.0088	0.0089	0.0084
Bone marrow	0.0153	0.013	0.0103	0.0106	0.0078
Tumor (5 mm)		0.034	0.04	0.044	0.04
Tumor (3 cm)		0.0066	0.0078	0.0085	0.0077

With the method described above, the percent uptakes of the injection dose per gram of tissue were measured for each location by correcting the physical half-life, the level of which was determined from the day of administration to the fifth day after injection. The results are shown in Table 1.

DISCUSSION

One of the promises that MoAb techniques offer is application to cancer therapy. To do this, it is necessary first to label the MoAb with a γ-ray emitting nuclide to determine the distribution within the body.[3,19] In this paper, we demonstrated our method of measurement and applied it to calculate the percentage of the injection dose per unit weight of the tumor, and of the liver and the bone marrow, which are thought to be critical organs during treatment.

It is obvious that SPECT is far superior to the planar method, in theory, for measuring the radioactive quantity accurately in a human body. However, in practice, SPECT might result in considerable error if sufficient care is not taken. In particular, the nonuniformity of the collimator and camera lead to noticeable error, because the reconstruction algorithm greatly emphasizes the nonuniformity. DeNardo et al. recommend SPECT, but the uptake obtained by the planar method was comparable with that by SPECT.[20] We think that SPECT provides the potential for greater accuracy; however, at present it is not clear which is better.

The estimation of the background counts involved in the ROI had considerable effect on the radioactive computation for the organ and the tumor. When activity in the liver was calculated on the assumption that there was no background activity in the liver ROI, uptake in the liver showed an increase of 39% over the value shown in Table 1. On the other hand, when we assumed that the background counts per pixel in the liver ROI were equal to the counts per pixel of the background ROI, uptake in the liver showed a 17% decrease over the value in Table 1. We measured the background counts involved in the organ ROI on the assumption that the shape of the subject's organ was the same as that of the average Japanese man[17] as expressed in a numerical formula. Actually, however, the shape of the subject's organ differed somewhat from that of the average man, and it was unlikely that the radioactivity of the background region was completely uniform. Accordingly, the estimation of the background counts might involve some degree of error.

Attenuation in the body was corrected with formula (1) or (2). The correction values AC1, AC2 and AC, were computed on the assumption that the shape of the subject's organ was the same as that of the average Japanese man, as was done for background subtraction, and that distributions of radioactivity in the organs and the tumor were uniform. However, the shape of the organ and the distribution of radioactivity in an actual patient differed somewhat from these assumptions. If the depth of the subject's organ differs by 1 cm from that of the average man, the correction value for attenuation causes 11% error, leading to $e^{0.1\times1}=1.11$, when using formula (2). Some error due to the attenuation correction might be involved.

We need to obtain accurate values for the organ and tumor volume in order to calculate the activity per gram of tissue. The estimation of organ volume has direct effects on the outcome of the calculation. In this paper, we used the values for the average Japanese man to estimate the liver and bone marrow uptakes. We calculated two types of models for the tumor, because there were numerous tumors of various sizes, ranging up to a diameter of 3 cm, and we could not measure the tumor thickness accurately by using external measurement, MRCT, XCT, or SPECT. Therefore, although a tumor 5 mm in diameter could not be detected, we calculated the upper bound of activity per gram of tissue on the assumption that the tumor would extend 5 mm below the skin, and the lowest bound on the assumption that the tumor would extend to a depth of 3 cm below the skin. The difference in tumor uptake per gram of tissue indicated in Table 1 was caused by the difference in the hypothesized volume of tumor. The actual activity per gram of tissue must be between these two computations.

Since MoAb is distributed in considerable amounts as a background throughout the whole body, the estimation of background counts involved in the ROI is very important. However, in general, the background counts were subtracted on the assumption that the background counts per pixel in the ROI were equal to the counts per pixel of the background ROI,[21] or no background subtraction was performed.[21,22] Therefore, the results obtained by these methods might involve a great degree of error. If the results of our estimation of liver uptake are applied as they are, the calculated value for uptake in the literature[21,22] would involve a -17% or $+39\%$ error when compared to the true value.

As for attenuation correction, it was mentioned in some reports as a method used in performing accurate correction when both anterior and posterior data were employed.[23] However, in general, the attenuation was corrected very roughly when one side data were used.[21,22,24] Our method corrected the attenuation accurately in both cases.

The goal of our research is to quantitatively measure the injected dose per gram of tissue for organs

and tumor. For this purpose, we have to measure the organ's weight, shape and location in each patient. In order to ensure that these data are correct, we have to perform a CT examination. In this case, it would be necessary to build a system consisting of a gamma camera, X-ray CT and computers, etc.

Even if it is decided that SPECT is superior to the planar method, the planar method would be available for the patient who is unable to undergo examination for a long time. In any case, background subtraction and attenuation compensation are indispensable for the planar method. We believe that our method, which computes background counts and the extent of attenuation by numerical integration, is useful in measuring the quantity of MoAb within each organ and in tumor.

ACKNOWLEDGEMENTS

The authors thank Prof. N. Arimizu and Dr. K. Uno of the Department of Radiology in the Chiba University School of Medicine, Dr. K. Murakami of the Department of Radiology in the National Sakura Hospital and Dr. M. Kobayashi of the Department of Dermatology in the Chiba University School of Medicine for their helpful suggestions and clinical assistance. They also thank Dr. S. Sakata of Chiba Cancer Center Hospital and Mr. J. Kubo and Mr. H. Aramata of Teijin Limited for their collaboration and support. This work was supported in part by a Grant-in Aid for Cancer Research, 62–17, from the Ministry of Health and Welfare, Japan.

REFERENCES

1. Humm JL: Dosimetric Aspects of Radiolabeled Antibodies for Tumor Therapy. *J Nucl Med* 27: 1490–1497, 1986
2. Cobb LM, Humm JL: Radioimmunotherapy of malignancy using antibody targeted radionuclides. *Br J Cancer* 54: 863–870, 1986
3. DeNardo GL, Raventos A, Hines HH, et al: Requirements for a Treatment Planning System for Radioimmunotherapy. *Int J Radiation Oncology Biol Phys* 11. 335–348, 1985
4. Groshar D, Frankel A, Iosilevsky G, et al: Quantitation of renal uptake of technetium-99m DSMA using SPECT. *J Nucl Med* 30: 246–250, 1989
5. Front D, Ioselevsky G, Frenkel A, et al: *In vivo* quantitation using SPECT of radiopharmaceutical uptake by human meningiomas. *Radiology* 164: 93–96, 1987
6. Schwinger RB, King MA, Doherty PW, Murray ME: Varidation of a Rotating Camera Based SPECT System for Dosimetry Applications. *J Nucl Med* 25: p 94, 1984
7. Budinger TF: Physical Attributes of Single-Photon Tomography. *J Nucl Med* 21: 579–592, 1980
8. Rogers WL, Clinthorne NH, Harkness BA, et al: Field-Flood Requirements for Emission Computed Tomography with an Anger Camera. *J Nucl Med* 23: 162–168, 1982
9. Sorenson JA: Quantitative Measurement of Radioactivity *in vivo* by Whole-Body Counting. In Instrumentation in Nuclear Medicine, Volume 2, Hine GJ and Sorenson JA, (ed.), New York, Academic Press, pp 311–348, 1974
10. Arimizu N, Morris AC: Quantitative Measurement of Radioactivity in Internal Organs by Area Scanning. *J Nucl Med* 10: 265–269, 1969
11. Graham LS, Neil R: *In vivo* Quantitation of Radioactivity using the Gamma Camera. *Radiology* 112: 441–442, 1974
12. Thomas SR, Maxon HR, Kereiakes JG: *In vivo* Quantitation of Lesion Radioactivity using External Counting Method. *Medical Physics* 3: 253–255, 1976
13. Thomas SR, Maxon HR, Kereiakes JG, et al: Quantitative Counting Techniques Enabling Improved Diagnostic and Therapeutic Decisions in Patients with Well-differentiated Thyroid Cancer. *Radiology* 122: 731–737, 1977
14. Shulkin BL, Sission JC, Koral KF, et al: Conjugate View Gamma Camera Method for Estimating Tumor Uptake of Iodine-131 Metaiodobenzylguanidine. *J Nucl Med* 29: 542–548, 1988
15. Hammond ND, Moldofsky PJ, Beardsley MR, et al: External Imaging Techniques for Quantitation of Distribution of I-131 F(ab')2 Fragments of Monoclonal Antibody in Humans. *Medical Physics* 11: 778–783, 1984
16. Wahl RL, Tuscan MC, Botti JM: Dynamic Variable Background Subtraction: A simple means of displaying radiolabeled monoclonal antibody scintigrams. *J Nucl Med* 27: 545–548, 1986
17. Yamaguchi H, Nishizawa K, Maruyama T, et al: A Computer Program to Calculate MIRD Tables for Japanese Physique. *Hoken Butsuri* 18: 43–48, 1983
18. Synder WS, Ford MR, Warner GG, Fisher HL: Estimation of Absorbed Fraction for Monoenergetic Photon Sources Uniformly Distributed in Various Organs of a Heterogeneous Phantom. *MIRD Pamphlet* No. 5: 1983
19. Iinuma TA: Recent Trend of Medical Imaging Technology—Emphasis of radionuclide imaging—. *RADIOISOTOPES* 36: 137–144, 1987
20. DeNardo GL, Macey DJ, DeNardo SJ, et al: Quantitative SPECT of Uptake of Monoclonal Antibodies. *Seminars in Nuclear Medicine* 19: 22–32, 1989
21. Macey DJ, DeNardo SJ, DeNardo GL, et al: Uptake of Indium-111-Labeled Monoclonal Antibody ZME-018 as a Function of Tumor Size in a Patient with Melanoma. *AMERICAN J PHYSIOLOGIC IMAGING* 3: 1–6, 1988
22. Taylor A, Milton W, Eyre H, et al: Radioimmunodetection of Human Melanoma with Indium-111-Labeled Monoclonal Antibody. *J Nucl Med* 29: 329–337, 1988
23. Eary JF, Appelbaum FL, Durack L, Brown P: Preliminary Validation of the Opposing View Method for Quantitative Gamma Camera Imaging. *Med. Phys* 16: 382–387, 1989

24. Keenan AM, Weinstein JN, Mulshine JL, et al: Immunolymphoscintigraphy in Patients with Lymphoma after Subcutaneous Injection of Indium-111-Labeled T101 Monoclonal Antibody. *J Nucl Med* 28: 42–46, 1987

Appendix 1

AC_1, AC_2, AC: Value used in correcting the attenuation in the body, C: Counts (cpm) from a whole part of an organ, O: Counts (cpm) per unit volume of organ before being attenuated by the body, l_1, l_2 $\cdots$, l_n: Path length from each part of the organ to a body surface, μ: Attenuation coefficient.

C can be expressed as follows:

$$C = O \cdot e^{-\mu l_1} + O \cdot e^{-\mu l_2} + \cdots + O \cdot e^{-\mu l_n}$$

Therefore O is as follows:

$$O = \frac{1}{e^{-\mu l_1} + e^{-\mu l_2} + \cdots + e^{-\mu l_n}} C$$

The total count in an organ is nO:

$$nO = \frac{n}{e^{-\mu l_1} + e^{-\mu l_2} + \cdots + e^{-\mu l_n}} C$$

Therefore correction values, AC_1, AC_2 and AC can be expressed as follows:

$$\frac{n}{e^{-\mu l_1} + e^{-\mu l_2} + \cdots + e^{-\mu l_n}}$$

This can be obtained easily with a personal computer.

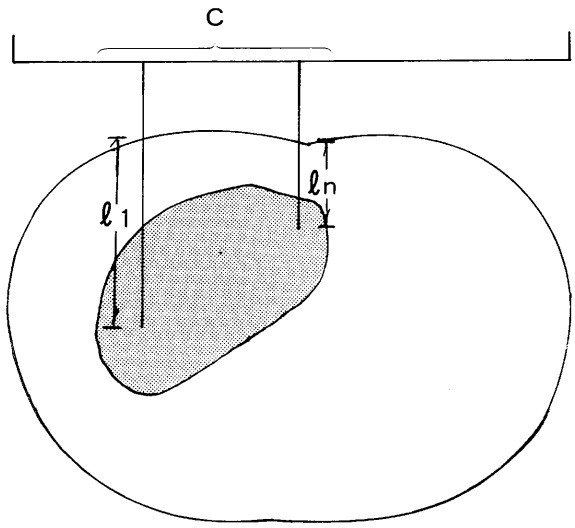

Appendix 1 Illustration explaining attenuation correction. It is assumed that the attenuation coefficient is uniform throughout the body, that the radioactive density in the organ is uniform, and that there is no radioactivity outside the organ. l_1, $\cdots$ and l_n are path lengths from each part of the organ to a body surface. C is counts (cpm) from a whole part of the organ.

Appendix 2

C_t: Counts (cpm) for the organ ROI, C_o: Background counts (cpm) included in the organ ROI, C_b: Counts (cpm) of the background ROI, P_o: Number of pixels for the organ ROI, P_b: Number of pixels for the background ROI, B: Background counts (cpm) per unit volume before being attenuated by the body, μ: Attenuation coefficient.

C_o and C_b can be expressed as follows:

$$\begin{aligned} C_o &= B(e^{-\mu lo_1} + e^{-\mu lo_2} + \cdots + e^{-\mu lo_n}) \\ C_b &= B(e^{-\mu lb_1} + e^{-\mu lb_2} + \cdots + e^{-\mu lb_m}) \end{aligned} \qquad \text{(A)}$$

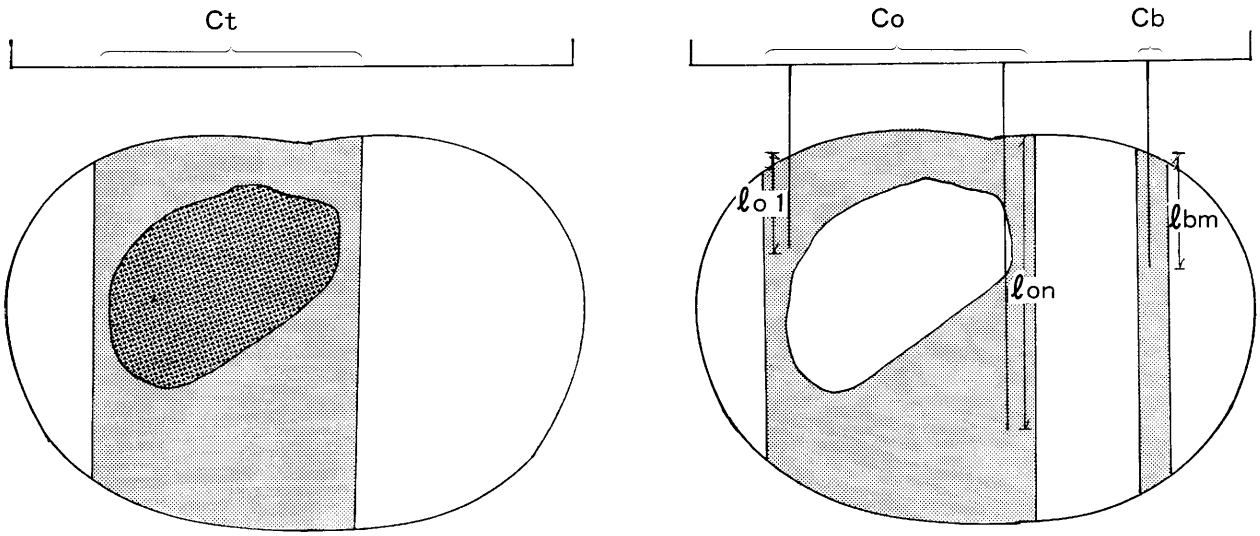

Appendix 2 Illustration to explain background subtraction. It is assumed that the attenuation coefficient is uniform throughout the body, and that the radioactive density in the background area is uniform. l_{o1}, $\cdots$ and l_{on} are path lengths from each part of the background to a body surface in the organ ROI, and l_{b1}, $\cdots$ and l_{bm} are those in the background ROI. C_t is counts (cpm) of the organ ROI, and C_b is that of the background ROI, respectively. C_o is background counts (cpm) included in the organ ROI.

The value of B is eliminated and the equation is rewritten as follows:

$$C_o = C_b \frac{P_o}{P_b} \left\{ \frac{(e^{-\mu lo_1} + e^{-\mu lo_2} + \cdots + e^{-\mu lo_n})/P_o}{(e^{-\mu lb_1} + e^{-\mu lb_2} + \cdots + e^{-\mu lb_m})/P_b} \right\} \quad \text{(B)}$$

The value in the brace is the ratio of the mean background count per pixel included in the organ ROI to that in the background ROI and it can be computed easily with a personal compnter. The not organ count, C, which is the ROI count after the background count is eliminated is as follows:

$$C = C_t - C_o$$